GSI Annual Report 2010 (extracts)

Average charges of heavy ions in a gas mixture

J. Khuyagbaatar[1], D. Ackermann[1], L.-L. Andersson[2,3], J. Ballof[4], Ch.E. Düllmann[1,4,5], J. Even[4], A. Gorshkov[6], R. Graeger[6], F.-P. Heßberger[1], W. Hartmann[1], D. Hild[4], R. Hoischen[2], A. Hübner[1], E. Jäger[1], B. Kindler[1], J.V. Kratz[4], J. Krier[1], S. Lahiri[7], B. Lommel[1], M. Maiti[7], E. Merchan[8], D. Rudolph[2], M. Schädel[1], H. Schaffner[1], B. Schausten[1], J. Steiner[1], A. Türler[4], A. Yakushev[1]

[1]GSI, Darmstadt, Germany; [2]Lund University, Lund, Sweden; [3]University of Liverpool, Liverpool, UK, [4]University of Mainz, Mainz, Germany; [5]HIM, Mainz, Germany; [6]Technical University München, Garching, Germany; [7]Saha Institute of Nuclear Physics, Kolkata, India; [8]Universidad Nacional de Colombia, Bogota, Colombia.

At present, gas-filled separators are typically filled with either pure helium (He) or pure hydrogen (H_2). Hydrogen seems to provide better suppression of background related to target-like ions [1]. However, as the average charges are lower than in pure He, a stronger dipole magnet is needed to separate evaporation residues. Therefore, at the gas-filled separator TASCA, experiments were performed with a fill-gas mixture of these two gases to investigate whether this allows for a combination of the advantages of the two gases, i.e., which allows a good suppression of the background while still keeping rather high average charges of evaporation residues. However, no data exists how to predict the average charges of heavy ions in gas mixtures. Thus, we aimed to study systematically average charges of heavy ions.

Earlier studies at TASCA clearly showed that the average charge is a function of the gas pressure [1]. This so called "density effect" was investigated on ^{252,254}No ions and a corresponding semi-empirical expression for the determination of the average charges was given in [1]. These expressions were used for the prediction of pressure dependent average charges of No ions in pure He and H_2. The experimental setup and the nuclear reactions used in the studies reported here are the same as in [1]. Magnetic rigidities were deduced as described in [2].

Measured magnetic rigidities of ^{254}No ions in the mixtures at certain relative amounts of the gases ν (He/H_2), are shown in Fig. 1 as a function of the pressure. Clearly, the "density effect" is observed also in the mixtures.

Charge equilibration of heavy ions moving in the gas is determined by a system of coupled homogeneous linear equations for fractions of each charge state and cross-sections of "charge-exchange" collisions (see [3] for details).

Let us assume that the charge equilibration is also occurring in gas mixtures, and that heavy ions (with initial charge state fractions of F_i) after the "charge-exchange" collisions have fractions F_i^{mix} ($\sum F_i^{mix} = 1$) for each i-th charge state. Each heavy ion with an i-th charge state has a probability $P_{He}=\nu/(\nu+1)$ and $P_{H2}=1/(\nu+1)$ to collide with either a He or a H_2 atom, respectively, with $P_{He}+P_{H2}=1$. Then, the fraction of each i-th charge state in gas mixtures can be written as: $F_i^{mix} = F_i \cdot P_{He} + F_i \cdot P_{H_2}$.

Average equilibrated charges in the gas mixtures can be derived as:

$$\bar{q}^{mix} = \sum q_i \cdot F_i^{mix} = \frac{\bar{q}^{He} \cdot \nu + \bar{q}^{H_2}}{\nu + 1}$$

where, q^{He} and q^{H2} are average charges of ^{254}No ions in pure He and H_2 at the same pressure as the gas mixture, respectively. Corresponding magnetic rigidities can be put into the following expression:

$$(B\rho)^{mix} = \frac{(B\rho)^{He} \cdot (B\rho)^{H_2} \cdot (1+\nu)}{(B\rho)^{He} \cdot (\upsilon/\upsilon_0)_{H_2} + (B\rho)^{H_2} \cdot (\upsilon/\upsilon_0)_{He} \cdot \nu} \cdot (\upsilon/\upsilon_0)_{mix}$$

where (υ/υ_0) with different indices are the velocities of the ^{254}No ions in different gases (He and H_2 cases are given in [2]). In our experiments: $(\upsilon/\upsilon_0)_{mix}$=2.39±0.03. Predicted magnetic rigidities from the above expression with $(\upsilon/\upsilon_0)_{mix}$=2.39 are shown in Fig. 1 by open dots. Experimental magnetic rigidities are well reproduced for ν=1 and 2, except for some underestimations at 0.8 mbar. Slightly underestimated magnetic rigidities were also observed in the case of ν=3 and 4. Again, in these cases gas pressures were 0.8 mbar. This discrepancy could be due to the linear function which was used to fit the observed "density effect" within the region (1-2) mbar in the case of pure H_2 [2]. More detailed information will be given in [4].

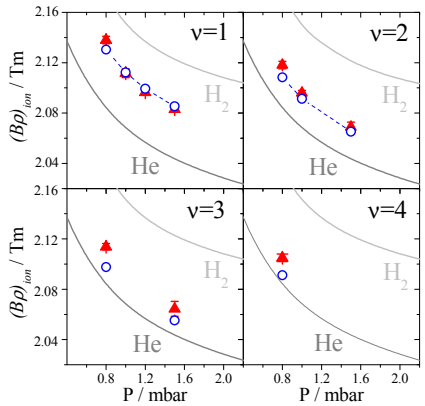

Figure 1: Magnetic rigidities of ^{254}No ions in gas mixtures ν depending on gas pressures P. Triangles and open circles are showing the measured and predicted magnetic rigidities, respectively. Lines are showing the fitted results for pure He and H_2 gases [1].

* These studies were financially supported the GSI F&E program and by the Research Center "Elementary Forces and Mathematical Foundations" (EMG).

[1] J. Khuyagbaatar et al., GSI Sci. Rep. 2009 (2010) 171.
[2] J. Khuyagbaatar et al., this GSI Sci. Rep.
[3] H.-D. Betz, Rev. Mod. Phys. 44 (1972) 465.
[4] J. Khuyagbaatar et al., to be published

Gas pressure influence on average charges of heavy recoils in TASCA

J. Khuyagbaatar[1], D. Ackermann[1], L.-L. Andersson[2,3], J. Ballof[4], W. Brüchle[1], Ch.E. Düllmann[1,4,5], J. Dvorak[5], K. Eberhardt[4], J. Even[4], A. Gorshkov[6], R. Graeger[6], W. Hartmann[1], F.-P. Heßberger[1], D. Hild[4], R. Hoischen[2], A. Hübner[1], E. Jäger[1], B. Kindler[1], J.V. Kratz[4], J. Krier[1], S. Lahiri[7], B. Lommel[1], M. Maiti[7], E. Merchan[8], D. Rudolph[2], M. Schädel[1], H. Schaffner[1], B. Schausten[1], E. Schimpf[1], A. Semchenkov[1,6], A. Serov[9], J. Steiner[1], A. Türler[4], A. Yakushev[1]

[1]GSI, Darmstadt, Germany; [2]Lund University, Lund, Sweden; [3]University of Liverpool, Liverpool, UK, [4]University of Mainz, Mainz, Germany; [5]HIM, Mainz, Germany; [6]Technical University München, Garching, Germany; [7]Saha Institute of Nuclear Physics, Kolkata, India; [8]Universidad Nacional de Colombia, Bogota, Colombia; [9]Paul Scherrer Intitute, Villigen, Switzerland

Several experimental works at gas-filled separators have been reported that lay the basis for a correct prediction of the average charges of heavy and superheavy ions [1-3]. These works resulted in differing semi-empirical parameterizations.

An interesting feature of heavy ion "charge-exchange" collisions is the so-called “density effect”, which has been observed at the Dubna gas-filled recoil separator DGFRS [2]. However, such an influence of the gas pressure has never been included in any of the above-mentioned semi-empirical expressions. The effect was also observed at the gas-filled separator TASCA [4]. Here we report results for ^{252,254}No ions which were produced in the fusion-evaporation reactions ^{48}Ca+^{206,208}Pb.

The experimental setup and the reactions were the same as in [4]. Average charges and magnetic rigidities of No ions were deduced using the experimental distribution of evaporation residues in a focal plane detector [4]. The analysis method was the same as in [3].

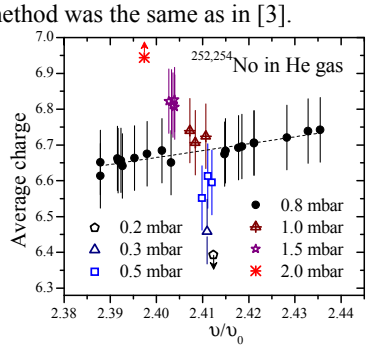

Figure 1: Measured average charges of the ^{252,254}No depending on their velocity (in units of the Bohr velocity). The line shows a linear fit. Arrows are marking limits for average charges.

Deduced average charges as a function of the velocity (expressed in units of the Bohr velocity, υ_0) are shown in Fig. 1. Average charges measured at 0.8 mbar gas pressure for both No ions (black solid dots) exhibit the linear dependence of the average charges on velocity. However, measured average charges at other pressures deviate significantly from this line. Deduced magnetic rigidities are shown in Fig. 2 for ^{252,254}No ions in helium (He) as well as for ^{254}No in hydrogen (H_2). These data show an increase of magnetic rigidities with decreasing pressure for both filling gases.

An expression to estimate the “density effect” has been given in [5] and we use it as a fit function for our experimental data. Average charges of heavy ions in a gas with pressure P can be presented as a sum of the equilibrated average charge and a correction term due to the "density effect", $q_{ion}=<q>+\Delta q$ [5]. Charge correction can be determined as as $\Delta q=a/(b+y)$ with $y=[(\upsilon/\upsilon_0)P]^{-1}$ according to [5]. The function $(B\rho)_{ion}=(c+dy)/(f+y)$ can be used to fit measured magnetic rigidities, with c,d and f being parameters.

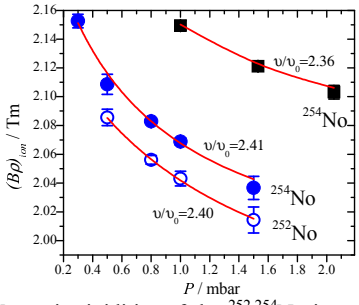

Figure 2: Magnetic rigidities of the ^{252,254}No ions as a function of the pressure. Circles and squares are denoting magnetic rigidities in He and H_2, respectively. Lines show fits to the data according to the relations given in the text.

Results of fits are shown in Fig. 2. The behavior of the fitted curves for both ^{252,254}No ions seems to be similar, as can be expected for ions with an identical atomic shell structure. The linear fit function $(B\rho)_{ion}= c+dy$ was used in the case of H_2 due to the limited number of experimental data points. These semi-empirical expressions which describe the “density effect” can be used as a correction for predicted average charges when using expressions from [1-3]. More detailed information will be provided in [6].

[1] A. Ghiorso., et al., NIM. A **269** (1988) 192.
[2] Yu. Oganessian et al., Phys. Rev. C **64** (2001) 064309.
[3] K.E. Gregorich et al., Phys. Rev. C **72** (2005) 014605.
[4] J. Khuyagbaatar et al., GSI Sci. Rep. 2009 (2010) 171.
[5] H.-D. Betz, Rev. Mod. Phys. **44** (1972) 465.
[6] J. Khuyagbaatar et al., to be published.

* These studies were financially supported the GSI F&E program and by the Research Center “Elementary Forces and Mathematical Foundations” (EMG).

Pulse Shape Analysis for the TASISpec Implantation Detector*

U. Forsberg[1], *P. Golubev*[1], *D. Rudolph*[1], *D. Ackermann*[2], *L.-L. Andersson*[3], *Ch.E. Düllmann*[2,4,5], *J. Even*[4], *J.M. Gates*[6], *J. Gellanki*[1], *F.P. Heßberger*[2,5], *R. Hoischen*[1,2], *E. Jäger*[2], *I. Kojouharov*[2], *J. Krier*[2], *N. Kurz*[2], *H. Schaffner*[2], *B. Schausten*[2], *M. Schädel*[2], *and A. Yakushev*[2]

[1]Lund University, Sweden; [2]GSI Helmholtzzentrum für Schwerionenforschung, Darmstadt, Germany; [3]University of Liverpool, UK; [4]Universität Mainz, Germany; [5]Helmholtz Institute Mainz, Germany; [6]Lawrence Berkely National Laboratory, USA

In TASISpec – TASCA in Small Image Mode Spectroscopy setup, which aims at decay spectroscopy of superheavy elements [1] – heavy ions are implanted into a double-sided silicon strip detector (DSSSD). Their subsequent decays are recorded in this, as well as in the surrounding silicon and germanium detectors. The use of sampling ADCs in the experimental setup open up for new possibilities, such as particle identification, as they allow for investigations of the actual pulse shapes from the detectors. Pulses from the DSSSD were integrated in charge-sensitive preamplifiers [2] and studied by splitting the signals between the standard electronics read-out chain and sampling ADCs (CAEN V1724) as shown in Fig. 1. The sampling ADCs digitise the pulses at a rate of 100 MHz. For each event, a time span of 2.56 μs around the arrival of the pulse was recorded and analysed offline. Triggers from the standard electronics were used. The accumulated data originates from a 3-line α source and an in-beam experiment in which the DSSSD was irradiated with heavy ions using the reaction ^{207}Pb(^{48}Ca,2n)^{253}No.

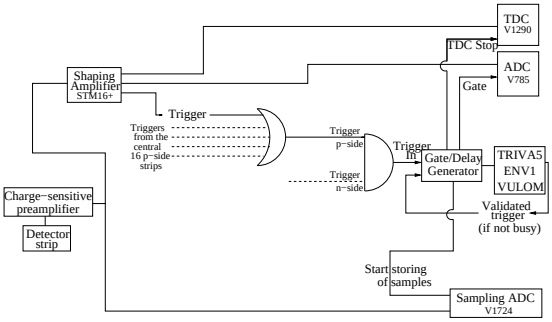

Figure 1: Electronics scheme for the DSSSD of TASISpec.

Any particle information present in the pulse shape resides within the rise of the pulse. The pulses were differentiated in order to emphasize this region of interest. Figure 2 shows the summed derivatives of pulses originating from the p-side (implantation side) of one pixel of the DSSSD; from α particles (red) and from implanted heavy ions (black). A difference between the pulse shapes appears in the "tail" of the derivative, which corresponds to the top of the original signal. This discrepancy was characterised by calculating the ratio of the integral over the particle-dependent area, and the integral of the main peak in the derivative. The regions used are marked in the figure.

* This work was supported by the Research Center "Elementary Forces and Mathematical Foundations".

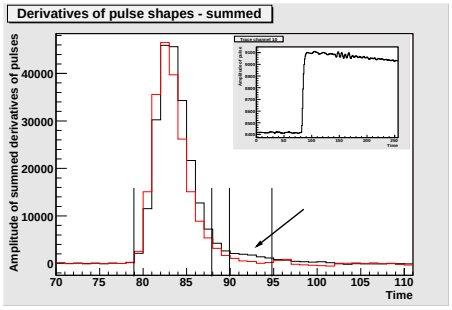

Figure 2: Summed derivatives of pulses from α particles (red) and implanted heavy ions (black). Insert: Typical pulse shape before software treatment.

The ratio between the two integrals was calculated for all pulses from the pixel, and the resulting distributions are shown in Fig. 3. The distribution from heavy ions is clearly shifted to the right compared to the one from α particles. Other pixels that were investigated show the same tendencies. This testifies that particle information is indeed present in the pulse shapes.

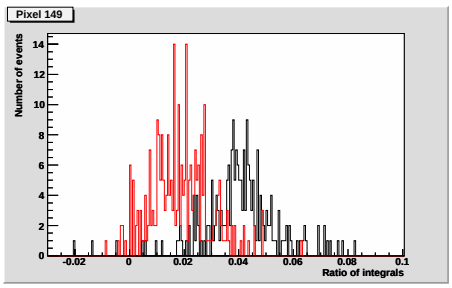

Figure 3: The ratio between the integrals for α particles (red) and implanted heavy ions (black).

In order to use the existing differences for a separation into α particles and implanted heavy ions, each strip, and possibly also every pixel, must be analysed individually in order to optimise the parameters used for the characterisation of the differences. This issue will be addressed in future analyses of pulse shapes from the TASISpec implantation detector.

References

[1] L.-L. Andersson *et al.*, Nucl. Instr. Meth. A **622**, 164 (2010)

[2] Ch. Görgen, G. Pascovici, Universität zu Köln

The control system for the new 100 mm target wheel at TASCA

T. Torres[1], E. Jäger[1] and J.Krier[1]

[1]GSI Helmholtzzentrum für Schwerionenforschung GmbH, Darmstadt, Germany;

A new target wheel system for the gas-filled separator TASCA with a 100 - mm diameter target wheel was designed and built. For this, a new motor control system was developed, basically consisting of a stepper motor [1], a stepper motor terminal [2], a control PC [2] and I/O terminals [2] for the input and output signals for the control loop.

The stepper motor terminal [2] is responsible to drive the motor in a controlled way, using a ramp function, up to the required frequency of 2250 revolutions per minute (rpm). The macro pulse signal (50 Hz HEAG signal) is connected to an input terminal and is used to synchronize the motor frequency to the HEAG signal. The exact wheel position (or more precisely the target position during the beam irradiation) is controlled and regulated using the master pulse (beam signal) as an input and the feedback of the wheel position at this time. To determine the wheel position during the 5 - ms long macropulse signal, (corresponding to the beam pulse) an optical position detection system was implemented. The system uses optical fiber sensors composed of the fiber units and the amplifier units [3]. Holes in the target wheel allow the laser to shine through when the wheel is at an exactly defined position: one set of holes generates a signal every 90° and the other one every 360°. These signals are connected to input terminals and processed for the control loop.

The implemented software [2] control system is based on the design and experience won with a similar system employing a large target wheel containing eight target segments used earlier at TASCA. It was designed and developed using the function principle of the finite state machine model, i.e., with the process being divided into states where each state has its input and output conditions. According to this, the transition to the next state (or if necessary to a previous state) will be given. Each state performs one or more functions required from the system. There is a principal task where this state is running and the additional tasks or subprograms (subroutines) which are called on each state as far as necessary. Defined states are implemented where the user has the possibility to stop the wheel movement; in this case the system will return to the initial state. Control functions are included to detect if there is an error present or if a movement function reports an error. Similar to the stop state, the error state is programmed to stop the axis movement in a very slow way with a ramp function, in order to protect the targets.

The setups required for the wheel movement like motor velocity, acceleration, beam cycle time, offset position from the master signal are preset such that the user is not required to enter these values.

As the used motor frequency of 2250 rpm is outside of the range of conventional stepper motor applications, there is the possibility that the motor fails to follow the rotation field and ends in a standing situation. Therefore a mechanism to detect the motor rotation or standing condition using the signal of the optical sensor system was implemented.

A user interface, divided into two areas was developed; in one window, the "operation window", the user is allowed to start or stop the movement and gets feedback information like the actual wheel movement status, the frequency of the wheel, if it is synchronous with the beam structure and error messages. The other one, the "service window", allows the user to change parameters for the synchronization of the master pulse to the target and includes other additional functions for improvements on the system development and maintenance.

The system was successfully tested with 5.5 MeV/u ^{24}Mg beam, in November 2010. Figure 1 shows an irradiated target wheel containing four tape targets to visualize the beam position. The beam hit each of the four targets at the correct position.

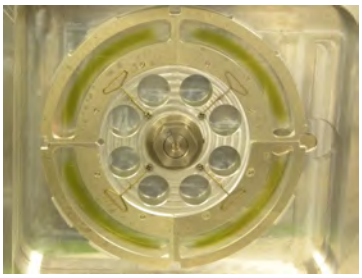

Figure 1: The new TASCA target wheel after a test irradiation with ^{24}Mg beam.

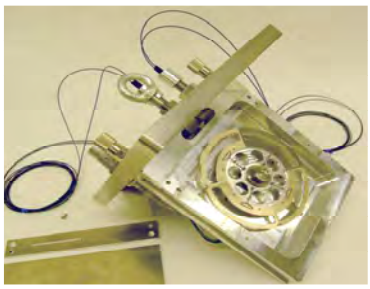

Figure 2: The complete assembly of the 100 mm target wheel in its cassette.

References

[1] High torque stepper motor ST5709X2508, Nanotec, www.nanotec.com

[2] Bus Terminals and TwinCAT software, Beckhoff, www.beckhoff.com

[3] Optical fiber sensors, OMRON, www.omron.com

Ion-optical simulations for the Inelastic Reaction Isotope Separator IRiS

J. Dvorak[1] and Ch. E. Düllmann[1,2,3]

[1]HIM, Mainz, Germany; [2]GSI, Darmstadt, Germany; [3]Institute für Kernchemie, Universität, Mainz, Germany.

Introduction

An impressive advancement in investigation of superheavy elements (SHE) was achieved in the past 25 years. The heaviest currently reported superheavy element contains 118 protons and novel challenging experiments pursuing the synthesis of elements 119 and 120 are under preparation. Yet all of these heaviest currently claimed elements were synthesized in nuclear fusion reactions, which can yield only neutron deficient products. Neutron-rich isotopes of the heaviest elements, which are of special interest e.g. in the context of nuclear chemistry and nuclear astrophysics, cannot be produced this way. The only viable production mechanism for neutron-rich nuclides is through multi-nucleon transfer reactions (MNTR), the application of which will give access to tens of new neutron-rich isotopes of the heaviest elements. Currently available separators are optimized for fusion products emitted under 0° and are poorly suited for MNTR studies due to their limited angular acceptance.

A new Inelastic Reaction Isotope Separator (IRiS) [1], dedicated to the investigation of neutron-rich isotopes of the heaviest elements produced in MNTR, will be constructed and set-up at the GSI in a joint effort of an international collaboration, headed by the Johannes Guttenberg University Mainz, the Helmholtz Institute Mainz, and the GSI Helmholtzzentrum für Schwerionenforschung Darmstadt. The main design goal of the IRiS is the ability to separate the heavy products formed in MNTR and deliver them to a focal plane. Here ion implantation and decay is detected in focal plane detector. To perform (i) chemical studies, (ii) mass measurements, and (iii) nuclear and atomic spectroscopy of the heavy ions separated in the IRiS, the detector setup will be retracted and allow the separated products to enter a gas cell, where they will be stopped and extracted for further investigation. A conceptual design scheme is shown in Fig. 1.

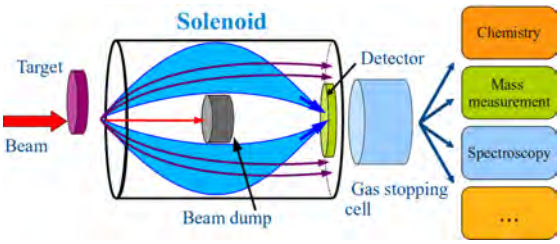

Figure 1: Schematic drawing of the IRiS design concept. Products are separated in a gas-filled solenoid magnet according to their magnetic rigidity. A beam dump stops the beam particles as well as 0° products.

Simulations

An essential part of the IRiS design process is the development of a computer simulation for the IRiS ion-optics. Due to the availability of theoretical predictions, the following two nuclear reactions were chosen as input for the simulation: ^{48}Ca+^{248}Cm at E_{CM}=209 MeV [2], and ^{238}U+^{248}Cm at E_{CM}=750 MeV [3]. The simulation code using the ROOT [4] framework is already highly advanced and includes: (i) Simulation of unreacted projectiles and products of elastic and inelastic scattering including MNTR; (ii) energy loss and straggling in the target; (iii) ion interaction with gas molecules and (iv) ion tracking in a realistic solenoidal magnetic field.

Simulation results

Simulations showed that relatively strong magnetic fields are necessary to achieve acceptable separation in a gas-filled solenoid. While several solenoid dimensions and magnetic field strengths were successfully tested, a stored energy of about 10 MJ was necessary in all cases. In symmetric ion-optical geometries, as shown in Fig. 2, efficiencies of typically about 20% for collecting the heaviest products ($Z \geq 102$) in the detector area were reached, while the detector count-rate due to background was estimated to about few kHz. Although not optimal for the identification of products in a focal plane detector, these conditions are well suited for use of a gas cell.

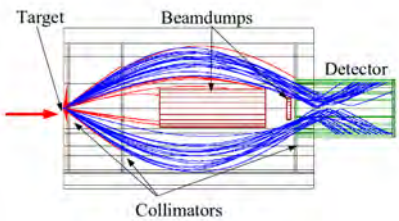

Figure 2: Trajectories of the heaviest products ($Z \geq 102$) produced in the reaction ^{48}Ca + ^{248}Cm.

Acknowledgements

C.E.D. acknowledges financial support from the Research Center “Elementary Forces and Mathematical Foundations” (EMG).

References

[1] J. Dvorak *et al.*, NIMA in press *http://dx.doi.org/10.1016/j.nima.2010.08.124*
[2] G.G. Adamian and N.V. Antonenko, private comm.
[3] V. Zagrebaev, private comm.
[4] ROOT- *http://root.cern.ch*

Prediction of Atomic Properties of Bi and Element 115

A. Borschevsky[1,2], V. Pershina[2], E. Eliav[3], and U. Kaldor[3]
[1]Massey University, Auckland, New Zealand; [2]GSI, Darmstadt, Germany; [3]Tel Aviv University, Israel

In this work, we perform fully relativistic benchmark calculations of polarizabilities (α), ionization potentials (IP), and electron affinities (EA) of element 115 and its lighter homologue, Bi. These properties are important for prediction of adsorption enthalpy (ΔH_{ads}) of the two elements on inert surfaces. Knowledge of ΔH_{ads} is required in order to guarantee the transport of the newly produced element from the target chamber to the chemistry set up. This is the first benchmark calculation of the polarizability of these elements.

Calculations of polarizabilities were performed using the DIRAC08 package [1], employing the finite field approach. In the Dirac-Coulomb (DC) *ab initio* method, the many-electron relativistic Dirac-Coulomb Hamiltonian

$$H_{DC} = \sum_i h_D + \sum_{i<j} 1/r_{ij} \qquad (1)$$

is employed, where

$$h_D = c\vec{\alpha}\cdot\vec{p} + \beta c^2 + V_{nuc}\,. \qquad (2)$$

The atomic orbitals (AO) are four-component spinors

$$\varphi_{nk} = \begin{pmatrix} P_{nk}(r) \\ Q_{nk}(r) \end{pmatrix}, \qquad (3)$$

where $P_{nk}(r)$ and $Q_{nk}(r)$ are the large and small component, respectively. The uncontracted Faegri basis set [2] was used for both atoms and extended to convergence with respect to the calculated polarizabilities. Electron correlation was taken into account at the Fock space coupled cluster level, FSCCSD. The contribution of the triple excitations and the higher order relativistic effects was also estimated. The ground state of both atoms is $^2P_{3/2}$, which, in the presence of an electric field, splits into $^2P_{3/2,1/2}$ and $^2P_{3/2,3/2}$. The final polarizabilities of the two states, together with the average polarizability $\alpha(^2P_{3/2})$, are presented in Table I.

IPs and EAs were calculated using the Dirac-Coulomb-Breit (DCB) Hamiltonian. Correlation was taken into account by Fock space coupled cluster method, augmented by intermediate Hamiltonian approaches [3,4] to facilitate convergence. The van der Walls radii (R_{vdW}) were determined from a linear correlation with $R_{max}(np_{1/2})$-AOs of the group 15 elements.

Chemistry of element 115 will be defined by its valence $7p_{3/2}$ orbital, which is destabilized and expanded due to relativistic effects, compared to that of Bi. Trends in atomic properties follow the trend set by the valence orbital. Element 115 will have the lowest ionization potential in the group, lower than that of Bi by almost 2 eV. The electron affinity will also be lowest in the group, reflecting the relativistic destabilization of the $7p_{3/2}$ orbital.

R_{vdW} of 115 is the highest in the group. There is also a steep increase in the average polarizability of the $^2P_{3/2}$ state from Bi to element 115, and the difference in the polarizability of the $^2P_{3/2,1/2}$ and $^2P_{3/2,3/2}$ states is much more significant in the superheavy homologue. This is again due to the relativistic destabilization and expansion of the $7p_{3/2}$ orbital.

Table 1. Atomic properties of Bi and element 115: IP (in eV), EA (in eV), α (in a.u.), and van der Walls radii, R_{vdW} (in Å)

Property	Value	Method	Ref
	Bi		
IP	7.303	DC+FSCC	this
	7.289	exp.	[6]
EA	1.015	DCB+FSCC	this
	0.942	exp.	[7]
$\alpha(^2P_{3/2,1/2})$	53.51	DC+FSCC	this
$\alpha(^2P_{3/2,3/2})$	41.20	DC+FSCC	this
$\alpha(^2P_{3/2})$	47.63	DC+FSCC	this
$\alpha(^2P_{3/2})$	48.6	CASPT2+LDA	[8]
R_{vdW}	2.33	corr.	this
	Element 115		
IP	5.553	DCB+FSCC	this
	5.579	DCB+FSCC	[9]
EA	0.368	DCB+FSCC	this
	0.383	DCB+FSCC	[9]
$\alpha(^2P_{3/2,1/2})$	100.20	DC+FSCC	this
$\alpha(^2P_{3/2,3/2})$	46.46	DC+FSCC	this
$\alpha(^2P_{3/2})$	73.69	DC+FSCC	this
R_{vdW}	2.46	corr.	this

References

[1] DIRAC08, written by H. J. Ja. Jensen *et al*. (2008)
[2] K. Faegri, Theor. Chim. Acta **105**, 252 (2001)
[3] A. Landau *et al.,* J. Chem. Phys. **121**, 6634 (2004)
[4] E. Eliav *et al.*, J. Chem. Phy. **122**, 224113 (2005)
[5] V. Pershina *et al*. J. Chem. Phys. **122** (2005) 124301
[6] C.E. Moore, *Atomic Energy Levels* (U.S. Goverment Printing Office, Washington, DC, 1958 (1958)
[7] T. Andersen *et al*, J. Phys. Chem. Rev. Data **28**, 1511(1999)
[8] B.O. Roos *et al.*, J. Phys. Chem. A **108**, 2851 (2004)
[9] E. Eliav *et al*., Mol. Phys. **94**, 181 (1998)

Relativistic *ab initio* Study on CnAu in Comparison with HgAu

A. Borschevsky[1,2], V. Pershina[2], E. Eliav[3], and U. Kaldor[3]
[1] Massey University, Auckland, New Zealand; [2] GSI, Darmstadt, Germany; [3] Tel Aviv University, Israel

Predictions of the interaction of the heaviest elements with various surfaces are essential for their transportation and identification in the gas-phase chromatography experiments. In an earlier work [1], we predicted the adsorption enthalpy, ΔH_{ads}, of element 112 (Cn) and its homolog Hg on inert surfaces (PE and Teflon) on the basis of the fully relativistic Dirac-Coulomb (DC) Fock space coupled cluster (FSCC) calculations of atomic properties. We have shown that Cn and Hg could be easily delivered from the target chamber to the chemistry set up due to their rather low $-\Delta H_{ads}$. In another work [2], we performed the 4-component Density Functional Theory (4c-DFT) calculations for the MAu_n systems (M = Hg and Cn, n = 1 – 120), in order to predict ΔH_{ads} of these elements on gold, which is used as a surface material for the detectors of the chromatography column. Since the DFT theory (though being applicable to large systems) is known to be less accurate than the *ab initio* DC coupled cluster approach (still being used only for small systems), we have performed these additional benchmark calculations for the MAu (M = Hg and Cn) dimers to be prove conclusions made on the basis of the DFT results.

We have employed the 4*c*-DC Hamiltonian,

$$H_{DC} = \sum_i h_D + \sum_{i<j} 1/r_{ij}, \quad (1)$$

where

$$h_D = c\vec{\alpha}\cdot\vec{p} + \beta c^2 + V_{nuc}. \quad (2)$$

V_{nuc} is the nuclear attraction operator, and α and β are the four-dimensional Dirac matrices. For computational efficiency, the exact 2c-relativistic Hamiltonian (X2C) approximation was used [3]. This is one of the most economical and accurate approximations to the 4c-DC Hamiltonian. Electron correlation was taken into account using the FSCC method, which is considered to be one of the most powerful tools in quantum chemistry. The calculations were performed using the DIRAC08 computational package [4]. The Faegri basis set was used [5], consisting of the 24*s*20*p*15*d*10*f*2*g* orbitals for Au and Hg and the 27*s*23*p*18*d*13*f*3*g* orbitals for Cn.

MAu (M = Hg and Cn) are open shell systems; hence we started our calculation with the closed shell reference state, MAu^-. After solving the Dirac-Coulomb equations and correlating the closed shell reference state, one electron was removed to obtain the neutral system, which was, in turn, re-correlated. Results of the calculations are given in Table 1 in comparison with our previous 4c-DFT ones [2] and those performed within various other approximations: relativistic effective core potentials (RECP) with spin-orbit (SO) corrections [6], pseudo-potentials (PP) combined with single double (triple) excitation CC method (CCSD(T)) [7], and other DFT results [6,8,9].

Table 1. Equilibrium bond lengths, R_e (in Å), dissociation energies, D_e (in eV), and vibrational frequencies, ω_e (in cm^{-1}) of HgAu and CnAu

R_e	D_e	ω_e	Method	Ref.
	HgAu			
2.635	0.46	119	DC+FSCC	this
2.653	0.53	116	ARECP+CCSD(T)+SO	[6]
2.711	0.39	103	PP+CCSD(T)	[7]
2.713	0.51	104	DFT+SO (B98)	[6]
2.791	0.41	93	DFT (B3LYP)	[8]
2.67	0.67	99	4c-DFT (B88/P86)	[2]
2.68	0.56	-	2c-DFT (PBE0)	[9]
2.68	0.62	-	2c-DFT (BP)	[9]
	CnAu			
2.700	0.42	98	DC+FSCC	this
2.727	0.39	95	ARECP+CCSD(T)+SO	[6]
2.774	0.36	83	DFT+SO (B98)	[6]
2.73	0.51	74	4c-DFT (B88/P86)	[2]
2.74	0.39	-	2c-DFT (PBE0)	[9]
2.73	0.47	-	2c-DFT (BP)	[9]

There is excellent agreement between the present *ab initio* DC values on the one hand and 4c-/ 2c-DFT ones on the other hand for R_e(MAu), while the DFT D_e(MAu) are systematically overestimated. Nevertheless, all the calculations come to the conclusion that Cn is less bound to Au than Hg. This is due to the strongest relativistic effects on the 7*s*(Cn) AO in group 12, making it less accessible for bonding than the 6*s*(Hg) AO. Thus, our results are in agreement with the expected trend. The next exciting task would be *ab initio* DC calculations of the 114-Au bonding in comparison with the Cn-Au one: element 114 is expected to be also very inert due to the stabilized $7p_{1/2}^2$ electron pair.

References

[1] V. Pershina, A. Borschevsky, E. Eliav and U. Kaldor, J. Chem. Phys **128**, 024707 (2008).
[2] V. Pershina *et al.* J. Chem. Phys., **131**, 084713 (2009).
[3] M. Iliaš and T. Saue, J. Chem. Phys. **126**, 064102 (2007).
[4] DIRAC 08, written by H. J. Ja. Jensen *et al*. (2008).
[5] K. Faegri, Theor. Chim. Acta **105**, 252 (2001).
[6] A. Zaitsevskii, *et al*. Cent. Eur. J. Phys. **4**, 448 (2006).
[7] R. Wesendrup and P. Schwerdtfeger, Angew. Chem. Int. Ed. **39**, 909 (2000).
[8] Z. J. Wu, Chem. Phys. Lett. **406**, 24 (2005).
[9] A. Zaitsevskii *et al*. J. Chem. Phys. **132**, 081102 (2010).

Novel Studies on the Electronic Structures and Volatility of MBr_5 (M = Nb, Ta, and Db)

V. Pershina[1], J. Anton[2], and T. Jacob[2]
[1]GSI, Darmstadt, Germany; [2]Institut für Elektrochemie, Universität Ulm, Germany

Many experimental studies were devoted in the past to the investigations of volatility of group 4 and 5 elements halides and oxyhalies [1]. Relativistic electronic structure theory rendered at that time assistance to those investigations by predicting molecular properties and trends in volatility [2]. Even though there was good agreement between the theory and experiment in the case of oxyhalides, there was a disagreement in the case of pure halides. Thus, e.g., theoretical predictions based on the 4*c*-DFT calculations of the electronic density distribution in the MBr_5 systems indicated higher volatility of $DbBr_5$ (as a vapour pressure over the solid) than their lighter homologs in the chemical groups [3], while experimentally, the following trend was observed: Nb ≈ Ta > Db [4].

To resolve this contradiction, new studies were undertaken both experimentally and theoretically. Experimentally, volatility of MBr_5 (M = Nb, Ta, and Db) was to be studied with the use of the isothermal gas-phase chromatography with a quartz column [5]. HBr was used as a reactive gas and KBr aerosol particles as a transport material. Theoretically, attempts to predict the behaviour of the MBr_5 species in these experiments were undertaken by us in this study on the basis of the state of art fully relativistic 4*c*-DFT calculations of the MBr_5 properties: Due to the latest development in the relativistic electronic structure theory, very accurate calculations of molecular properties such as dissociation energies and optimized geometries (bond lengths) become possible [6], which was not the case 20 years ago.

For prediction of adsorption of MBr_5 on the quartz surface of the chromatography column, the following scenarios were considered: i) physisorption of MBr_5 on the (brominated) SiO_2 surface; ii) formation of the $KMBr_6$ salt on the surface; iii) formation and adsorption of $MOBr_3$; iv) the $(Si_sO)_2MBr_3$ formation on the surface. In this report, we present results of the calculations of properties of the MBr_5 molecules and their adsorption according to the first scenario, which turned out to be the most appropriate.

The total energy calculations have shown the MBr_5 formation to obey the following trend: $NbBr_5 < TaBr_5 < DbBr_5$. The calculated properties of MBr_5, needed for predictions of ΔH_{ads} via the physisorption model

$$E(x) = -\frac{3}{16}\left(\frac{\varepsilon - 1}{\varepsilon + 2}\right)\frac{\alpha_{at}}{\left(\frac{1}{IP_{slab}} + \frac{1}{IP_{at}}\right)x^3}, \qquad (1)$$

where IP is the ionization potential, α is the polarizability, x is the molecule-surface distance and ε is the dielectric constant of the adsorbent material, are given in Table I.

Table 1. Ionization potentials, IP (in eV), polarizabilities, α (in a.u.), equilibrium bond lengths, R_e (in Å), interaction distance, x (in Å), and adsorption enthalpies, $-\Delta H_{ads}$ (in kJ/mol), of MBr_5 (M = Nb, Ta, and Db)

Property	$NbBr_5$	$TaBr_5$	$DbBr_5$
IP	9.35	9.33	9.37
α_x	159.1	155.6	157.3
α_y	167.6	157.4	156.6
α_z	200.8	188.1	187.6
$<\alpha>$	175.8	167.0	167.1
R_e(ax/eq)	2.500/2.448	2.495/2.442	2.550/2.496
R_e(ax/eq)*	-	2.473/2.412	-
x	2.794	2.779	2.799

* Experimental values

Using the data of Table 1, $-\Delta H_{ads}$ of MBr_5 on the pure SiO_2 (ε = 2.81) and brominated with KBr (estimated ε = 5.1) quartz surfaces were predicted. The results are given in Table 2.

Table 2. Adsorption enthalpies, $-\Delta H_{ads}$ (in kJ/mol), of MBr_5 (M = Nb, Ta, and Db) on quartz surface

$-\Delta H_{ads}$	$NbBr_5$	$TaBr_5$	$DbBr_5$
on SiO_2, calc.	66	64	62
on SiO_2-KBr, calc.	77	75	73
experiment [5]	89 ± 5	101 ± 5	-

According to the present calculations, volatility of $DbBr_5$ should be higher than that of $NbBr_5$ and $TaBr_5$, though the differences in ΔH_{ads} between the species should be very small. This is in agreement with the earlier predictions [3]. The obtained trend is in reasonable agreement with the results on $NbBr_5$ and $TaBr_5$ [4,5] taking into account the experimental error bars. (The absolute values cannot be really compared due to the unknown value of ε). The predicted lower volatility of $DbBr_5$ in comparison with that of the homologs has been confirmed by results of the very recent gas-phase isothermal chromatography experiments [5].

References

[1] H. W. Gäggeler, A. Türler, In: The Chemistry of Superheavy Elements, Ed. M. Schädel, Kluwer, 2003, pp. 237-290.
[2] V. Pershina, Chem. Rev. **96** (1995) 1977.
[3] V. Pershina, *et al*. J. Chem. Phys. **98** (1992) 1116.
[4] H. W. Gäggeler, *et al*. Radiochim. Acta **57** (1992) 93.
[5] Qin Zhi, private communication.
[6] J. Anton, *et al*. Phys. Rev. A **69** (2004) 012505.

Towards fully-relativistic simulations of the adsorption of super-heavy elements on α-SiO_2 surfaces *

W. Gao[1], *Ch. E. Düllmann*[1,3,4], *J. Anton*[2], *T. Jacob*[2], *and V. Pershina*[3]

[1]Institut für Kernchemie, Universität Mainz, Germany; [2]Institut für Elektrochemie, Universität Ulm, Germany; [3]GSI Helmholtz-Zentrum für Schwerionenforschung, Darmstadt, Germany; [4]Helmholtz Institut Mainz, Germany

While in the last two decades super-heavy elements with $Z \leq 112$ have been studied, the focus of the present work is on the chemical properties of element 114. Our theoretical calculations have been motivated by two conflicting gas-chromatography experiments, which aimed on studying the interaction strength of element 114 with a gold surface. The experiment by Eichler *et al.* [1] reported adsorption in the chromatography column at only very low temperatures of approximately $-90\,^{\circ}\mathrm{C}$, from which they concluded a weak interaction between element 114 and the gold surface. In contrast, experiments performed at GSI [2] observed adsorption at room temperature, indicating a much stronger bond between element 114 and gold. To resolve this conflict further experiments will be performed at GSI within the next two years, where besides gold SiO_2 will be used as detector material.

Besides the previously mentioned experiments, extensive theoretical studies on the adsorption of element 114 on gold surfaces were performed using fully-relativistic DFT methods [3], while the adsorption on inert surfaces such as SiO_2 were estimated using semi-empirical methods in conjunction with computed properties of atoms, dimers, or small molecules [3, 4]. Unfortunately a fully-relativistic treatment of the entire adsorption process is beyond the capacities of nowadays computing ressources. However, this work can be divided into two steps: (i) extensive studies on SiO_2 bulk and surface properties (e.g. stable bulk-phases or possible surface structures and terminations) using a non-relativistic approach; (ii) fully-relativistic calculations on the adsorption process of element 114 on SiO_2, where the most stable and interesting surface structures obtained in the first step serve as basis.

So far we have focused on the first task, understanding the surface structure of SiO_2 under realistic experimental conditions. For these calculations, the CASTEP code [6] with Vanderbilt-type ultrasoft pseudopotentials [7] and the PBE exchange–correlation functional has been used. The obtained DFT-energies were then used in conjunction with the *ab initio* atomistic thermodynamics approach [5] to evaluate the surface phase diagrams, providing information of the surface stability as function of surrounding temperature and pressure. Starting with bulk systems, our calculations show that at experimental conditions ($p_{O_2} = 10^{-13}$ atm, $100\,\mathrm{K} < T < 320\,\mathrm{K}$) the most stable bulk structure is the so called α-quartz. Using this crystal structure as basis, various surface orientations and morphologies were studied. We find that the thermodynamically preferred structure is the α-SiO_2(001) surface, which could assume three different morphologies: one Si-terminated and two different O-terminated structures.

Figure 1 shows the surface free energy, $\gamma(p,T)$, for the most stable surface structures as function of the oxygen chemical potential. Structure **a**, which is Si-terminated, is favored at $\Delta\mu_O < -6.24\,\mathrm{eV}$ ($T \gg 1000\,\mathrm{K}$ under UHV conditions). In the temperature range until $\sim$100 K the surface is O-terminated (structure **b**). The phase diagram shows the existence of a fourth, but less stable structure (structure **d**), which is terminated by a single O-layer.

After understanding the surface morphology of SiO_2 under experimental conditions, the next step will be to perform fully-relativistic DFT calculations on the actual adsorption process of elements 112 and 114 and their homologs on a α-SiO_2(001) surface (structure **b**).

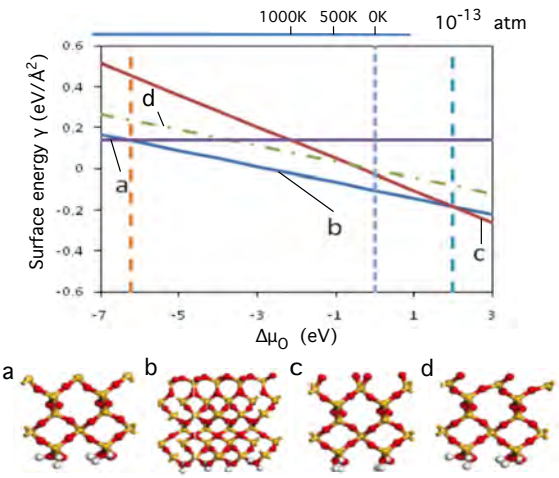

Figure 1: Surface free energy of the α-SiO_2(001) as function of $\Delta\mu_O$ or temperature at fixed pressure of 10^{-13} atm.

References

[1] R. Eichler *et al.*, Radiochim Acta **98** (2010) 133.

[2] A. Yakushev *et al.*, this Scientific Report.

[3] V. Pershina, J. Anton, and T. Jacob, J. Chem. Phys. **131** (2009) 084713.

[4] V. Pershina, T. Bastug, and B. Fricke, J. Chem. Phys. **122** (2005) 124301.

[5] K. Reuter and M. Scheffler, Phys. Rev. B **65** (2002) 035406.

[6] M. D. Segall *et al.*, J. Phys.: Condens. Matter **14** (2002) 2717.

[7] D. Vanderbilt, Phys. Rev. B **41** (1990) 7892.

* This work was supported by the Research Center "Elementary Forces and Mathematical Foundations" (EMG)